

High-Performance Photoinduced Memory with Ultrafast Charge Transfer Based on MoS₂/SWCNTs Network Van Der Waals Heterostructure

Zhenyu Yang, Hao Hong, Fang Liu, Yuan Liu, Meng Su, Hao Huang, Kaihui Liu, Xuelei Liang, Woo Jong Yu, Quoc An Vu, Xingqiang Liu, and Lei Liao*

Photoinduced memory devices with fast program/erase operations are crucial for modern communication technology, especially for high-throughput data storage and transfer. Although some photoinduced memories based on 2D materials have already demonstrated desirable performance, the program/erase speed is still limited to hundreds of micro-seconds. A high-speed photoinduced memory based on MoS₂/single-walled carbon nanotubes (SWCNTs) network mixed-dimensional van der Waals heterostructure is demonstrated here. An intrinsic ultrafast charge transfer occurs at the heterostructure interface between MoS₂ and SWCNTs (below 50 fs), therefore enabling a record program/erase speed of $\approx 32/0.4$ ms, which is faster than that of the previous reports. Furthermore, benefiting from the unique device structure and material properties, while achieving high-speed program/erase operation, the device can simultaneously obtain high program/erase ratio ($\approx 10^6$), appropriate storage time ($\approx 10^3$ s), record-breaking detectivity ($\approx 10^{16}$ Jones) and multibit storage capacity with a simple program/erase operation. It even has a potential application as a flexible optoelectronic device. Therefore, the designed concept here opens an avenue for high-throughput fast data communications.

on bulk semiconductors are already approaching their fundamental physical limits, and cannot meet the needs for wearable, flexible, and transparent technologies. 2D materials are considered as an excellent platform for next-generation optoelectronic devices, benefiting from the unique optoelectronic properties and excellent compatibility with well-established silicon technologies.^[1–9] Moreover, van der Waals heterostructure provides a way to feasibly select and stack different 2D materials with sharp interface for various functional devices, avoiding the challenge of lattice mismatch.^[5–9]

By exploiting the atomically thin 2D materials, several novel photoinduced memory devices have demonstrated inspiring performances in recent years.^[10–16] A heterostructure between graphene and MoS₂ has exhibited a rewritable photoinduced memory.^[10] Monolayer MoS₂ with artificial charge traps is also used as an photoinduced memory with long storage time ($\approx 10^4$ s) and multibit optical storage state.^[11] Few-layers MoS₂/PbS heterostructure can even detect and store the infrared signal.^[12] Until recently, a multibit photoinduced memory based on WSe₂/BN heterostructure is reported, demonstrating a high program/erase ratio

1. Introduction

Photoinduced memory devices are used to detect and store optical signal, which are crucial component for data communications. Conventional photoinduced memory devices based

Dr. Z. Yang, Dr. M. Su, Dr. H. Huang, Prof. L. Liao
State Key Laboratory for Chemo/Biosensing and Chemometrics
School of Physics and Technology
Wuhan University
Wuhan 430072, China
E-mail: liaolei@whu.edu.cn

Dr. H. Hong, Prof. K. Liu
State Key Laboratory for Mesoscopic Physics
Collaborative Innovation Centre of Quantum Matter
School of Physics
Peking University
Beijing 100871, China

Dr. F. Liu, Prof. X. Liang
Key Laboratory for the Physics and Chemistry of Nanodevices
and Department of Electronics
Peking University
Beijing 100871, China

Prof. Y. Liu, Prof. X. Liu, Prof. L. Liao
Key Laboratory for Micro-/Nano-Optoelectronic
Devices of Ministry of Education
School of Physics and Electronics
Hunan University
Changsha 410082, China

Prof. W. J. Yu
Department of Electrical and Computer Engineering
Sungkyunkwan University
Suwon 16419, Korea

Dr. Q. A. Vu
IBS Center for Integrated Nanostructure Physics
Institute for Basic Science
Sungkyunkwan University
Suwon 16419, Korea

DOI: 10.1002/sml.201804661

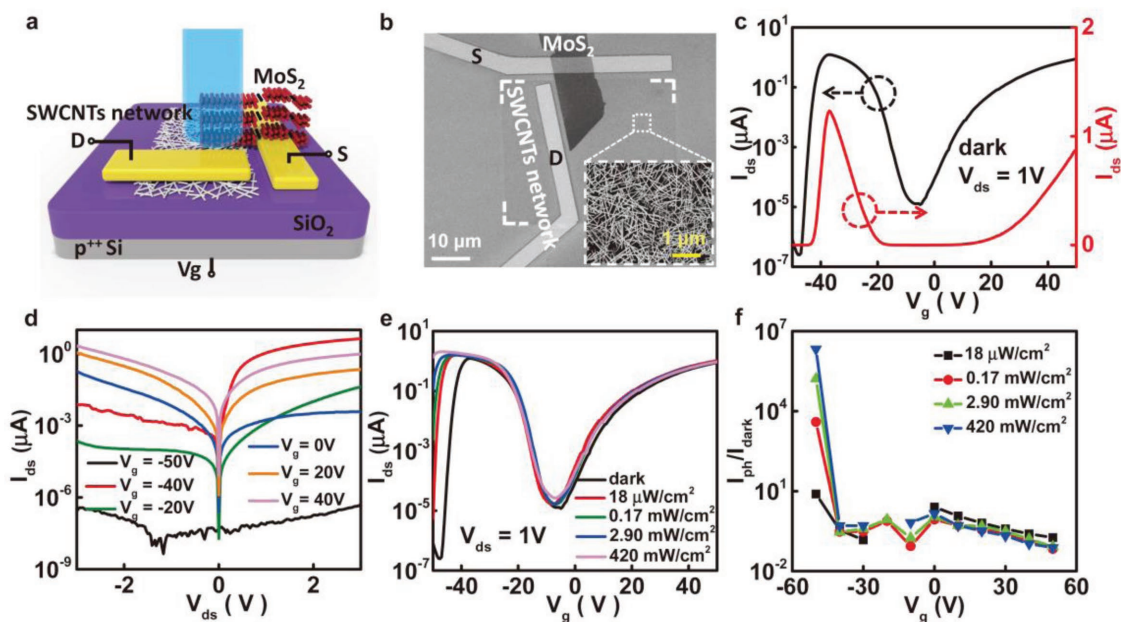


Figure 1. Schematic illustration and optoelectronic properties of the photoinduced memory device. a) The schematic and b) the SEM image of the device based on MoS₂/SWCNTs network heterostructure on 300 nm SiO₂/Si substrate. The inset of (b) displays the morphology and density of SWCNTs network. The scales are 10 and 1 μm, respectively. c) The transfer characteristic and d) the output characteristic curve of the device in dark. e) The change of the drain source current (I_{ds}) with different laser intensity. f) The ratio of photocurrent (I_{ph}) to dark current (I_{dark}) with different gate voltage.

($\approx 10^7$).^[15] However, these previous studies largely ignore the program/erase speed, which plays an important role in optical communication technology with high-throughput fast data storage and transfer. Moreover, because of limitations of material properties, their performance cannot meet all the needs of ideal photoinduced memories at the same time, including fast program/erase speed, high program/erase ratio, simple program/erase operation and appropriate storage time at room temperature.

Here, due to an ultrafast charge transfer (below 50 fs) at the MoS₂/single-walled carbon nanotube (SWCNT) interface, we demonstrate a high-speed photoinduced memory device based on the MoS₂/SWCNTs network mixed-dimensional van der Waals heterostructure. The program/erase time in the photoinduced memory device is only $\approx 32/0.4$ ms, which is two orders of magnitudes faster than that of previous reports based on 2D/2D material heterostructure photoinduced memory device.^[10–12] In addition, combining the unique device structure and material properties, the heterostructure device can obtain a high program/erase ratio ($\approx 10^6$). And by controlling the behavior of trapped photogenerated carrier in the SWCNTs network, the MoS₂/SWCNTs network mixed-dimensional heterostructure device achieves an appropriate storage time ($\approx 10^3$ s) and has the multibit storage capacity (≈ 10 optical storage states) with a simple program/erase operation. At the same time, the device also displays a record ultrahigh D^* ($\approx 10^{16}$ Jones) as a photodetector in 2D materials heterostructure device, and it even can stay on the good optoelectronic property on the flexible substrate, which has certain guiding significance for future flexible photoinduced memory devices.

2. Results and Discussion

2.1. Fabrication and Electrical Characterization of the Heterostructure Device

Figure 1a displays the schematic image of the photoinduced memory device based on MoS₂/SWCNTs network mixed-dimensional heterostructure. The uniform SWCNTs network is obtained by directly dip coating the SWCNTs solution (see Experimental Section) onto the 300 nm SiO₂/p⁺⁺-Si substrate and its bandgap is about 0.6 eV.^[17] Then a reactive ion etching is introduced to pattern the network into isolated stripes, which can efficiently suppress the leakage current. Subsequently, the source electrode (30 nm Au) is patterned near the edge of the SWCNTs network stripes. And then mechanically exfoliated multilayer MoS₂ is simultaneously transferred onto the top of SWCNTs network stripe and the predefined source electrode using the physical transfer method,^[18] to form a high-quality and trap-free interface between MoS₂ and SWCNTs network.^[10] The predefined source electrode using top contact to MoS₂ can avoid the associated chemical disorder and defect-induced gap states at the MoS₂/Au electrode interface.^[19] Finally, the other drain electrode is defined on the SWCNTs network at the edge of MoS₂. Typical scanning electron microscopy (SEM) image of the device is shown in Figure 1b, and the inset displays the morphology and density of SWCNTs network. To make a tradeoff of current and on-off ratio, few-layer MoS₂ (≈ 10 nm) is selected as the light absorption layer with the visible range bandgap (1.2 eV),^[10,20–22] and the corresponding atomic force microscopy is shown in Figure S1 in the Supporting Information.

The transfer and output characteristics of the fabricated device are shown in Figure 1c,d, both of which demonstrate sharp changes with V_g . Note that it even presents a novel “N” curve in the transfer characteristic (Figure 1c). Correspondingly, when the V_g changes from negative to positive, the output characteristic also displays three different states (Figure 1d). Applying a large negative V_g (≈ -50 V) to the gate, the carriers in MoS₂ are completely depleted (Figure S2a, Supporting Information), due to the material properties of MoS₂ and the negligible electric field shielding of SWCNTs network with its natural hole structure. Hence, there is no current flowing through the MoS₂/SWCNTs network mixed-dimensional heterostructure. As the V_g increases to the range of -40 to -20 V, MoS₂ is working at its subthreshold region. In the meantime, the SWCNTs network exhibits p-type characteristics (Figure S2c, Supporting Information). The device forms a p–n heterojunction, resulting in forward conduction and good rectification characteristic. Further increasing the V_g to ≈ -10 V, the SWCNTs network becomes nonconductive (Figure S2c, Supporting Information). The current is suppressed by SWCNTs network and cannot flow though the mixed-dimensional heterostructure again. At last when the V_g is further increased to positive range, multilayer MoS₂ and SWCNTs network both exhibit n-type properties, so the device changes to an n–n heterojunction. In this case, the device is conductive in both direction and the rectification characteristic disappears.

Figure 1e presents the change of drain source current (I_{ds}) with a 532 nm incident laser under various power density. The heterostructure device gains a high ratio of photocurrent (I_{ph}) and dark current (I_{dark}), which reaches up to 10^7 at the negative V_g (-50 V) in Figure 1f. It is a foundation of the good optoelectronic device. Unless otherwise emphasized, the illumination light is a 532 nm laser, and all tests are performed at room temperature.

2.2. Mechanism of the Photoinduced Memory Device

Figure 2a presents the working processes of the device. As the laser (421 mW cm^{-2}) turns on, I_{ds} rapidly increases to a maximum value, which is the process of program optical signal. When laser is turned off, I_{ds} still maintains a large current in dark, indicating that the device can effectively store previous optical signal. Finally, the positive V_g pulse (50 V) is used to erase the storage optical signal and the device can return to a nonconductive initial state. So this is a complete dynamic working process of the photoinduced memory device, including program, storage, and erase optical signal. The duration of the laser pulse and the positive V_g pulse both are 0.1 s.

Figure 2b–d discusses the working mechanism of the photoinduced memory device in detail. As aforementioned, when a large negative V_g (≈ -50 V) is applied to the device,

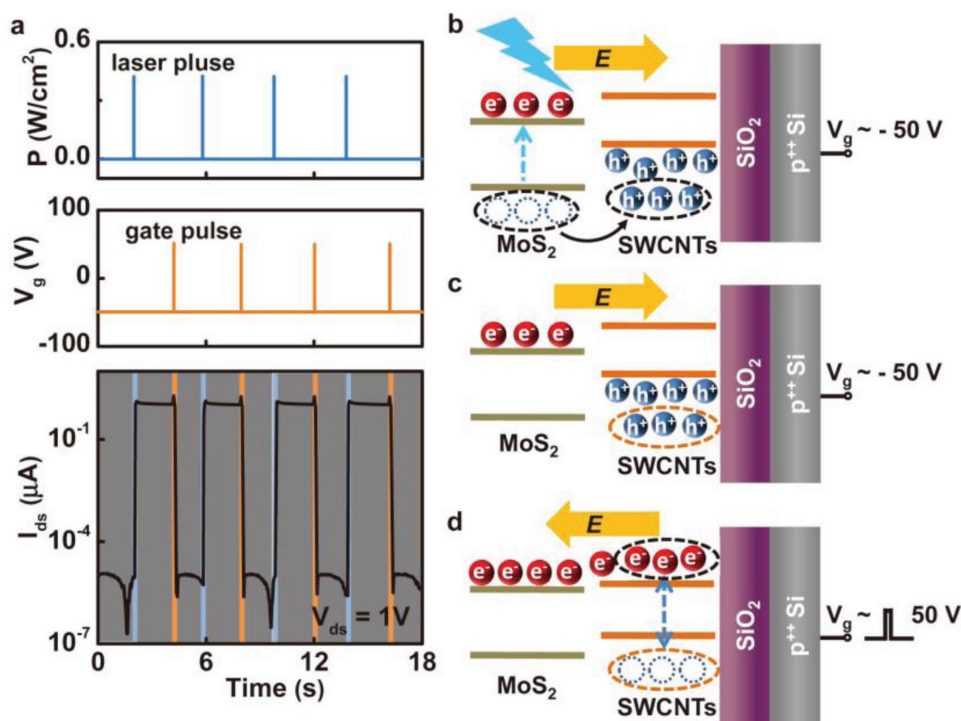


Figure 2. Work process and mechanism explanation of the photoinduced memory device. a) The program, storage, and erase process of the photoinduced memory device using laser pulses and V_g pulses, respectively. The blue curve represents the laser pulse, which is 421 mW cm^{-2} with a duration of 0.1 s. The orange curve is a V_g pulse, which is 50 V and a duration of 0.1 s. The shade of gray indicates a dark environment, the shade of blue indicates the program process with a laser pulse, and the shade of orange indicates the erase process with a V_g pulse. b) The mechanism of program process. The black-dotted frame displays that the photogenerated holes are transferred to the SWCNTs network under the electric field. c) The mechanism of storage process. The orange-dotted frame represents charge traps at the SWCNTs network. d) The mechanism of erase process. The trapped holes recombine with the excess electrons under the positive V_g .

the memory device is initially nonconductive under dark condition. Once the laser turns on as shown in Figure 2b, the MoS₂ can absorb photonic energy to generate a large number of electron–hole pairs, because of the strong optical absorption and strong light–matter interactions (Figure S3, Supporting Information).^[1,10,23,24] Then, the photogenerated holes of MoS₂ can simply enter the SWCNTs network under a negative electric field through the high-quality and trap-free interface between MoS₂ and SWCNTs network. Finally, because there are stable charge traps in the SWCNTs network, which originates from the water or hydroxyl groups on polar substrate surfaces (such as glass or SiO₂),^[17,25–27] the photogenerated holes are effectively trapped into the charge traps of the SWCNTs network under a negative electric force. This can prevent the recombination of photogenerated electron–hole pairs. Therefore, large amounts of photogenerated electrons are accumulated in MoS₂ layer.^[10,11] In addition, the trapped photogenerated holes in the SWCNTs network can also screen and weaken the negative electric field in MoS₂ layer.^[10,11] So even if a negative V_g (–50 V) is applied, the MoS₂ can demonstrate a large electron current at this time. Combined with p-type SWCNTs network, the device will form a p–n junction under light condition. So high current density is shown in the photoinduced memory device, where the optical signal is programmed in the device.

As the laser is turned off, it is difficult for photogenerated holes to escape from the traps of SWCNTs network with a negative electric force (Figure 2c), where only few photogenerated holes can recombine with the photogenerated electrons in the MoS₂ in dark condition. Plenty of photogenerated electrons are still accumulated in the MoS₂, and photogenerated holes continue to screen and weaken the negative electric field in MoS₂ layer. Hence, the photoinduced memory device keeps conductive in dark condition, leading to the state of storage optical signal.

A positive V_g (50 V) pulse is applied to the device to erase the low-resistance state of the device. Under a positive V_g, MoS₂ and SWCNTs both become n-type conductive. The previously trapped holes in the SWCNTs can be released through the recombination with the excess electron as shown in Figure 2d. Meanwhile the gate screening effect also disappears, due to the recombination of trapped holes in the SWCNTs network. So after a positive V_g pulse ends, the MoS₂ will become nonconductive under the negative V_g. And the device recovers to the nonconductive state, which is the process of erase optical signal in the mixed-dimensional heterostructure memory device.

2.3. Performance of the Photoinduced Memory Device

Compared with other 2D/2D heterostructure photoinduced memories, the screen effect is negligible in the MoS₂/SWCNTs network heterojunction device due to lots of natural hole structure in SWCNTs network. So when the V_g is applied –50 V, the MoS₂ become complete depletion and the SWCNTs networks has large p-type current, which combine to bring about the high program/erase ratio. As shown in Figure 2a, the photoinduced memory device has a high program/erase ratio, which can reach to ≈10⁶. It is close to the reported maximum program/erase ratio.^[14] The storage time is also more than 10³ s in the photoinduced memory device (Figure 3a). During the storage process, the current is negligibly changed, reflecting a good retention characteristic. As the storage mechanism described above (Figure 2c), the stable charge traps in SWCNTs network effectively capture photogenerated hole and prevents photogenerated hole from recombining with photogenerated electron, which results in a constant conductivity in dark condition. In order to obtain the longer storage time, there are two types of possible optimization solutions: the functionalization of the

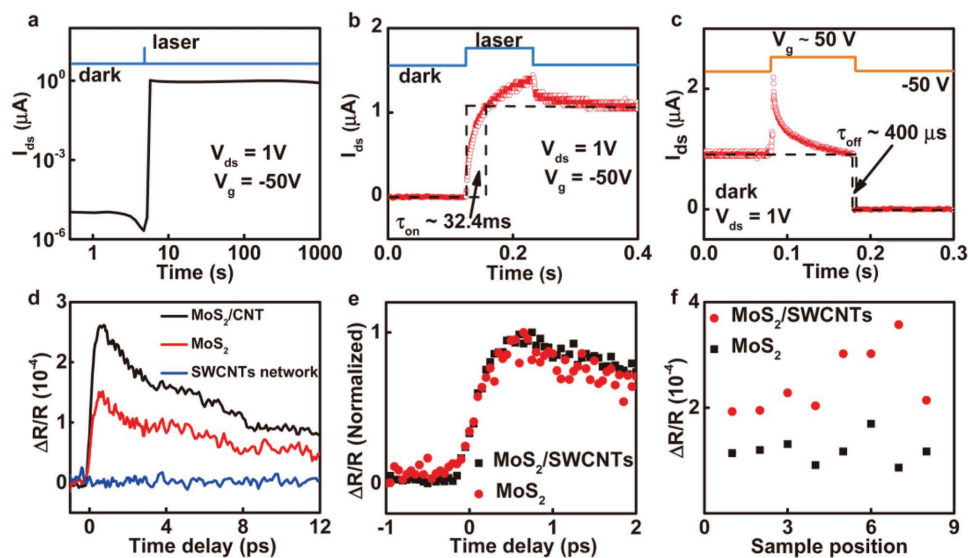


Figure 3. The program, storage, and erase performance in the photoinduced memory device. a) The storage time of the photoinduced memory device. b) The speed of program process. c) The speed of erase process. d) Time-resolved transient absorption signals of MoS₂/SWCNTs heterostructure, pristine MoS₂, and pristine SWCNTs based on the pump-probe with the resonance pump of 670 nm and the probe of 820 nm. e) The normalized transient absorption signal. f) Transient absorption test in different locations of the sample.

oxide dielectric interfaces introducing more artificial charge traps or inserting h-BN to form MoS₂/h-BN/SWCNTs structure to prevent charge leakage. Figure 3b,c displays a high-speed program/erase operation in the photoinduced memory device, which is 32 and 0.4 ms, respectively. It is two orders of magnitudes faster than previous reports based on other 2D/2D material heterostructure photoinduced memories.^[10–12]

The high speed of program/erase operation results from an intrinsic ultrafast charge transfer at the mixed-dimensional heterostructure interface between MoS₂ and SWCNTs. To identify the limitation of charge transfer, an ultrafast pump-probe experiment is applied with resonance pump at 670 nm and probe at 820 nm. Time-resolved transient absorption signals of pristine MoS₂, pristine SWCNTs, and the mixed-dimensional heterostructure of MoS₂/SWCNTs, are respectively shown in Figure 3d. When the pump-probe is applied in the pristine SWCNTs, there is no obvious transient absorption signal, consistent with our experiment that SWCNTs network is not sensitive to visible light (Figure S3b, Supporting Information). Comparing the heterostructure signal with that of pristine MoS₂, two significant features unambiguously reveal the ultrafast interfacial charge transfer in the mixed-dimensional heterostructure of MoS₂/SWCNTs. Firstly, the heterostructure signal is enhanced by ≈1.5 times (Figure 3d). The enhanced signal is from the transferred carriers, as previous works reported.^[28,29] Secondly, the rise-up curve of heterostructure and pristine MoS₂ is almost the same fast, according to the normalized transient absorption signal in Figure 3e. Since only after charge transfer the transient absorption signal of heterostructure can be enhanced, the charge transfer time is convoluted in the rise-up curve. Therefore, the identical rise rate indicates that interfacial charge transfer time-scale is already less than our experiment resolution of ≈50 fs,^[29,30] corresponding an intrinsic bandwidth up to THz. Finally, transient absorption test is performed in different locations of the sample and all of them give out the same results (Figure 3f).

The ultrafast charge transfer is the result of two unique advantages in MoS₂/SWCNTs device geometry. First, the strong interlayer electronic coupling and the presence of valence band offset contribute to the ultrafast charge transfer in the mixed-dimensional heterostructure.^[29,31] Because the more electronic states overlap, the easier it is to redistribute carriers. Second, due to a typical bipolar in SWCNTs network, the Fermi level of SWCNTs can be greatly tuned by an external V_g to enable a nearly transparent band alignment with MoS₂, similar to the contact between graphene and MoS₂,^[32] and it is also beneficial to the ultrafast charge transfer. On the other hand, by the finite element analysis method, the contact of cylinder surface to plane can generate a stronger electric field at the line contact interface under same source drain voltage (V_{ds}) (Figure S4, Supporting Information). Therefore, compared with other 2D/2D material heterostructure, a stronger electric field makes easier for carriers to pass through the interface, further decreasing the required time of program/erase operation. All these things lead to the higher program/erase speed (32/0.4 ms) than other 2D/2D heterostructure photoinduced memories.

To demonstrate the good stability of the photoinduced memory, Figure 4a shows a repeatable program/erase switch of 200 cycles. Even though the light source is a common mobile phone flash, flashlight, or light-emitting diode in everyday life, the photoinduced memory device still performs well in the process of program, storage, and erase optical signal (Figure 4b). This further indicates the photoinduced memory has excellent weak light responsiveness. Figure 4c shows the multibit optical signal storage property in the device. A laser pulse (≈19.3 mW cm⁻²) represents an optical signal, where the illumination duration of the laser pulses is 0.1 s. And the time interval between two laser pulses is about 2 s. With increasing the number of laser pulse, the readout current evenly rises. The device distinctly exhibits ten optical storage states defined as “0,” “1,” and up to “9.” In addition, the readout current can be

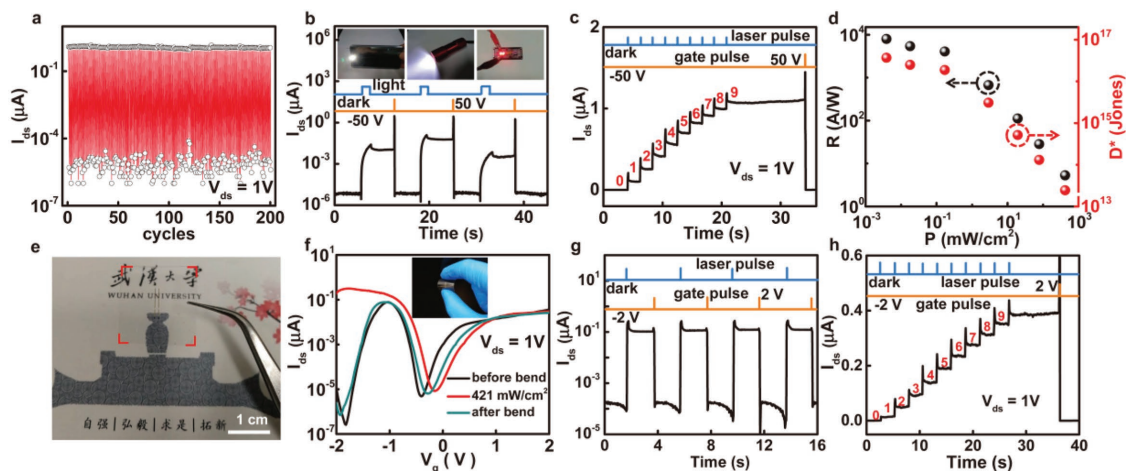


Figure 4. Reliability test and practical application of the photoinduced memory device. a) The reliability test based on the program/erase switch of 200 cycles. b) The performance of the photoinduced memory device using a common mobile phone flash, flashlight, or light-emitting diode. c) The multibit storage property in the device. Ten states which are defined “0,” “1,” up to “9” are continuously programmed by multiple laser pulses. The intensity of the 532 nm laser is 19.3 mW cm⁻² and its duration of 0.1 s. The readout current can be erased by a positive gate voltage pulse. d) The performance of the device as a photodetector. e) Photograph of the device on the flexible PET substrate with 30/5 nm HfO₂/SiO₂ dielectric. The scale is 1 cm. f) Corresponding photoelectric properties of the device on the PET substrate. g) The storage display of the photoinduced memory device on the flexible PET substrate. h) The multibit storage property of the photoinduced memory device on the flexible PET substrate.

kept relatively stable for an appropriate time until it is erased by the positive V_g pulse (50 V) to restore the initial state. The excellent multibit memory phenomena displays that it can be used in optoelectronic multibit logic devices.

Based on the mechanism of program optical signal described above, the MoS₂/SWCNTs network heterostructure device can also be used as a photodetector under a negative V_g (−50 V). In the output characteristic curve, the current increases rapidly with the laser intensity increasing (Figure S5, Supporting Information). According to change of output current, some important performance parameters is extracted as a photodetector, such as the photoresponsivity (R) and the detectivity (D^*) in Figure 4d.

The R is calculated by the formula, $R = I_{ph}/PA$.^[6,13,14] The P is the power density of laser illumination, and the A is the device area. The R of the device can reach $8 \times 10^3 \text{ A W}^{-1}$ at $V_{ds} = 3 \text{ V}$ and under the low laser intensity of $4 \mu\text{W cm}^{-2}$, which is comparable to other heterojunction photodetectors.^[8,13,14] Because the shot noise resulting from dark current is the main limiting factor for detectivity,^[6,33] the D^* can be calculated as $D^* = RA^{1/2}/(2eI_{dark})^{1/2}$, where the e is the electron charge. Due to the ultrahigh I_{ph}/I_{dark} ratio, the D^* is up to 10^{16} in the photoinduced memory device. To the best of our knowledge, it is the highest of all relevant reports reported for photodetector based on 2D materials heterostructure.^[12,34–36] The ultrahigh D^* shows that the device has a good performance as a photodetector.

Finally, the performance of the device on the flexible PET substrate is shown. Figure 4e is the photo image of MoS₂/SWCNTs network heterostructure device on the PET substrate. A metal gate is firstly deposited on the PET substrate, and then a 30 nm HfO₂ is grown by atomic layer deposition, and it continues to grow 5 nm SiO₂ on the HfO₂ by electron beam sputtering. The 30 nm HfO₂ and 5 nm SiO₂ are used together as a gate dielectric. The HfO₂ is used to improve the level of gate leakage, and 5 nm SiO₂ is used to generate the charge traps at the interface between CNTs and SiO₂. Finally, the heterostructure device is fabricated on the HfO₂/SiO₂ dielectric layer, as the method described above. The device still has an excellent optoelectronic property on the PET substrate, even if the PET substrate is bent (Figure 4f). Besides, the device can program, store, and erase the store optical signal on the flexible PET substrate with 30/5 nm HfO₂/SiO₂ dielectric (Figure 4g). And it also can keep the multibit optical signal storage property on the flexible PET substrate (Figure 4h). However, after multiple bends, the storage performance of the device is significantly degraded, and even breakdown leakage is likely to occur. This requires us to explore more suitable flexible substrate to improve the stability of our memory device in the future.

3. Conclusion

In summary, we have demonstrated a high-speed photoinduced memory device based on the MoS₂/SWCNTs network mixed-dimensional heterostructure. Due to the ultrafast charge transfer between MoS₂ and SWCNTs network (below 50 fs), the photoinduced memory device exhibits the highest program/erase speed at room temperature so far ($\approx 32/0.4$ ms). It has a significant impact on the optical communication technology

for the high-throughput data transfer. Moreover, by taking full advantage of the material and structural properties, the device shows a high program/erase ratio ($\approx 10^6$), appropriate storage time ($\approx 10^3$ s), and the multibit storage capacity (≈ 10 optical storage states) with a simple program/erase operation. The device also shows an excellent optoelectronic property with a record-breaking detectivity ($\approx 10^{16}$ Jones) in 2D materials heterostructure devices and it even can work on the flexible substrate. Such great performance represents that the device has a potential in the next-generation photoinduced memory devices.

4. Experimental Section

Material Preparation and Device Fabrication: The MoS₂ bulk crystal was purchased from SPI Company. High purity (>99%) semiconducting SWCNTs solution was prepared according to the method of Gu et al.^[37] The average diameter of the SWCNTs was about 1.4 nm. The SWCNTs were dispersed in chloroform, with the concentration of $10 \mu\text{g mL}^{-1}$. Highly uniform SWCNT thin films were fabricated by dip coating adapted from Dong et al.^[38] The electron beam lithography (JEOL 6510 with NPGS system) was employed to pattern the electrodes. Au was thermal evaporated as the contact electrodes, followed by liftoff. In addition, the HfO₂ on the flexible PET substrate was grown with KE-MICRO TALD-200A under a low temperature of 95 °C.

Measurement Conditions: The optoelectronic measurements of the device were mainly carried out on the Lake Shore TTPX probe station, with Agilent B1500A and B2912A semiconductor parameter analyzer. The high program/erase speed was measured using a preamplifier (Model SR570 of Stanford research systems) and Agilent DSO-X2022A digital storage oscilloscope with a 532 nm laser illumination.

Supporting Information

Supporting Information is available from the Wiley Online Library or from the author.

Acknowledgements

Z.Y. and H.H. contributed equally to this work. This work was supported by the National Key Research and Development Program of Ministry of Science and Technology (Grant No. 2018YFB0406603), NSFC grant (Nos. 61811540408, 61625401, 61574101, and U1632156), the Strategic Priority Research Program of Chinese Academy of Sciences (Grant No. XDB30000000), as well as the Natural Science Foundation of Hunan Province (Nos. 2017RS3021 and 2017JJ3033).

Conflict of Interest

The authors declare no conflict of interest.

Keywords

photoinduced memory, program/erase performance, ultrafast charge transfer, van der Waals heterostructures

Received: November 7, 2018

Revised: November 24, 2018

Published online: December 13, 2018

- [1] J. Yin, Z. Tan, H. Hong, J. Wu, H. Yuan, Y. Liu, C. Chen, C. Tan, F. Yao, T. Li, Y. Chen, Z. Liu, K. Liu, H. Peng, *Nat. Commun.* **2018**, *9*, 3311.
- [2] X. Zhou, L. Gan, W. Tian, Q. Zhang, S. Jin, H. Li, Y. Bando, D. Golberg, T. Zhai, *Adv. Mater.* **2015**, *27*, 8035.
- [3] J. Quereda, P. San-Jose, V. Parente, L. Vaquero-Garzon, A. J. Molina-Mendoza, N. Agrait, G. Rubio-Bollinger, F. Guinea, R. Roldan, A. Castellanos-Gomez, *Nano Lett.* **2016**, *16*, 2931.
- [4] Z. Li, Y. Li, T. Han, X. Wang, Y. Yu, B. Tay, Z. Liu, Z. Fang, *ACS Nano* **2017**, *11*, 1165.
- [5] R. Cheng, F. Wang, L. Yin, Z. Wang, Y. Wen, T. A. Shifa, J. He, *Nat. Electron.* **2018**, *1*, 356.
- [6] Z. Yang, L. Liao, F. Gong, F. Wang, Z. Wang, X. Liu, X. Xiao, W. Hu, J. He, X. Duan, *Nano Energy* **2018**, *49*, 103.
- [7] D. Li, M. Chen, Z. Sun, P. Yu, Z. Liu, P. M. Ajayan, Z. Zhang, *Nat. Nanotechnol.* **2017**, *12*, 901.
- [8] Q. A. Vu, J. H. Lee, V. L. Nguyen, Y. S. Shin, S. C. Lim, K. Lee, J. Heo, S. Park, K. Kim, Y. H. Lee, W. J. Yu, *Nano Lett.* **2017**, *17*, 453.
- [9] M. Massicotte, P. Schmidt, F. Violla, K. Watanabe, T. Taniguchi, K. J. Tielrooij, F. H. Koppens, *Nat. Commun.* **2016**, *7*, 12174.
- [10] K. Roy, M. Padmanabhan, S. Goswami, T. P. Sai, G. Ramalingam, S. Raghavan, A. Ghosh, *Nat. Nanotechnol.* **2013**, *8*, 826.
- [11] J. Lee, S. Pak, Y. W. Lee, Y. Cho, J. Hong, P. Giraud, H. S. Shin, S. M. Morris, J. I. Sohn, S. Cha, J. M. Kim, *Nat. Commun.* **2017**, *8*, 14734.
- [12] Q. S. Wang, Y. Wen, K. M. Cai, R. Q. Cheng, L. Yin, Y. Zhang, J. Li, Z. X. Wang, F. Wang, F. M. Wang, T. A. Shifa, C. Jiang, H. Yang, J. He, *Sci. Adv.* **2018**, *4*, eaap7916.
- [13] S. Jang, E. Hwang, Y. Lee, S. Lee, J. H. Cho, *Nano Lett.* **2015**, *15*, 2542.
- [14] D. Lee, E. Hwang, Y. Lee, Y. Choi, J. S. Kim, S. Lee, J. H. Cho, *Adv. Mater.* **2016**, *28*, 9196.
- [15] D. Xiang, T. Liu, J. Xu, J. Y. Tan, Z. Hu, B. Lei, Y. Zheng, J. Wu, A. H. C. Neto, L. Liu, W. Chen, *Nat. Commun.* **2018**, *9*, 2966.
- [16] Y. J. Jeong, D. J. Yun, S. H. Noh, C. E. Park, J. Jang, *ACS Nano* **2018**, *12*, 7701.
- [17] Q. K. Qian, G. H. Li, Y. H. Jin, J. K. Liu, Y. Zou, K. L. Jiang, S. S. Fan, Q. Q. Li, *ACS Nano* **2014**, *8*, 9597.
- [18] F. Gong, H. Fang, P. Wang, M. Su, Q. Li, J. C. Ho, X. Chen, W. Lu, L. Liao, J. Wang, W. Hu, *Nanotechnology* **2017**, *28*, 484002.
- [19] Y. Liu, J. Guo, E. Zhu, L. Liao, S. J. Lee, M. Ding, I. Shakir, V. Gambin, Y. Huang, X. Duan, *Nature* **2018**, *557*, 696.
- [20] X. Zou, J. Wang, C. H. Chiu, Y. Wu, X. Xiao, C. Jiang, W. W. Wu, L. Mai, T. Chen, J. Li, J. C. Ho, L. Liao, *Adv. Mater.* **2014**, *26*, 6255.
- [21] J. Wang, Q. Yao, C. W. Huang, X. Zou, L. Liao, S. Chen, Z. Fan, K. Zhang, W. Wu, X. Xiao, C. Jiang, W. W. Wu, *Adv. Mater.* **2016**, *28*, 8302.
- [22] Z. Yang, X. Liu, X. Zou, J. Wang, C. Ma, C. Jiang, J. C. Ho, C. Pan, X. Xiao, J. Xiong, L. Liao, *Adv. Funct. Mater.* **2017**, *27*, 1602250.
- [23] L. Britnell, R. M. Ribeiro, A. Eckmann, R. Jalil, B. D. Belle, A. Mishchenko, Y. J. Kim, R. V. Gorbachev, T. Georgiou, S. V. Morozov, A. N. Grigorenko, A. K. Geim, C. Casiraghi, A. H. Castro Neto, K. S. Novoselov, *Science* **2013**, *340*, 1311.
- [24] K. F. Mak, J. Shan, *Nat. Photonics* **2016**, *10*, 216.
- [25] S. Schneider, M. Brohmann, R. Lorenz, Y. J. Hofstetter, M. Rother, E. Sauter, M. Zharnikov, Y. Vaynzof, H. J. Himmel, J. Zaumseil, *ACS Nano* **2018**, *12*, 5895.
- [26] C. M. Aguirre, P. L. Levesque, M. Paillet, F. Lapointe, B. C. St-Antoine, P. Desjardins, R. Martel, *Adv. Mater.* **2009**, *21*, 3087.
- [27] W. Kim, A. Javey, O. Vermesh, O. Wang, Y. M. Li, H. J. Dai, *Nano Lett.* **2003**, *3*, 193.
- [28] J. He, N. Kumar, M. Z. Bellus, H. Y. Chiu, D. He, Y. Wang, H. Zhao, *Nat. Commun.* **2014**, *5*, 5622.
- [29] X. Hong, J. Kim, S. F. Shi, Y. Zhang, C. Jin, Y. Sun, S. Tongay, J. Wu, Y. Zhang, F. Wang, *Nat. Nanotechnol.* **2014**, *9*, 682.
- [30] Z. Ji, H. Hong, J. Zhang, Q. Zhang, W. Huang, T. Cao, R. Qiao, C. Liu, J. Liang, C. Jin, L. Jiao, K. Shi, S. Meng, K. Liu, *ACS Nano* **2017**, *11*, 12020.
- [31] J. Zhang, H. Hong, J. Zhang, H. Fu, P. You, J. Lischner, K. Liu, E. Kaxiras, S. Meng, *Nano Lett.* **2018**, *18*, 6057.
- [32] Y. Liu, H. Wu, H. C. Cheng, S. Yang, E. Zhu, Q. He, M. Ding, D. Li, J. Guo, N. O. Weiss, Y. Huang, X. Duan, *Nano Lett.* **2015**, *15*, 3030.
- [33] X. Liu, L. Gu, Q. Zhang, J. Wu, Y. Long, Z. Fan, *Nat. Commun.* **2014**, *5*, 4007.
- [34] F. Wang, Z. Wang, K. Xu, F. Wang, Q. Wang, Y. Huang, L. Yin, J. He, *Nano Lett.* **2015**, *15*, 7558.
- [35] M. Long, E. Liu, P. Wang, A. Gao, H. Xia, W. Luo, B. Wang, J. Zeng, Y. Fu, K. Xu, W. Zhou, Y. Lv, S. Yao, M. Lu, Y. Chen, Z. Ni, Y. You, X. Zhang, S. Qin, Y. Shi, W. Hu, D. Xing, F. Miao, *Nano Lett.* **2016**, *16*, 2254.
- [36] W. Yu, S. Li, Y. Zhang, W. Ma, T. Sun, J. Yuan, K. Fu, Q. Bao, *Small* **2017**, *13*, 1700268.
- [37] J. Gu, J. Han, D. Liu, X. Yu, L. Kang, S. Qiu, H. Jin, H. Li, Q. Li, J. Zhang, *Small* **2016**, *12*, 4993.
- [38] G. Dong, J. Zhao, L. Shen, J. Xia, H. Meng, W. Yu, Q. Huang, H. Han, X. Liang, L. Peng, *Nano Res.* **2018**, *11*, 4356.